www.czasopisma.pan.pl PAN POLSKA AKADEMIA NAUK www.journals.pan.pl

A R C H I V E S O F M E T A L L U R G Y A N D M A T E R I A L S

Volume 58 2013 Issue 2

DOI: 10.2478/amm-2013-0010

A. KUKUŁA-KURZYNIEC*, J. DUTKIEWICZ*, P. OCHIN**, L. PERRIÈRE**, P. DŁUŻEWSKI***, A. GÓRAL*

AMORPHOUS - NANOCRYSTALLINE MELT SPUN Al-Si-Ni BASED ALLOYS MODIFIED WITH Cu AND Zr

AMORFICZNO-NANOKRYSTALICZNE ODLEWANE TAŚMY Al-Si-Ni MODYFIKOWANE Cu I Zr

In the present paper glass forming ability and structure of Al-Si-Ni based alloys were investigated. Three alloys starting from the ternary $Al_{78}Si_{12}Ni_{10}$ [alloy 1], $Al_{75}Si_{12}Ni_8Zr_5$ [alloy 2] and $Al_{73}Si_5Ni_7Cu_8Zr_7$ [alloy 3] were subjected to melt spinning process. The mean thickness of the obtained ribbons amounted between 25 and 40 μm. XRD and DSC studies showed predominantly amorphous structure of the ribbons. STEM and HRTEM methods confirmed participation of crystalline phase identified mainly as Al solid solution with the grain size near 10 nm. The mean microhardness [0.1N] of the ribbons was measured for alloys 1 – 3 respectively: 457 HV, 369 HV and 536 HV. The high value of hardness can be related to the presence of α-Al dispersoids in the amorphous matrix.

Keywords: AlSiNi base metallic glass, melt spinning, amorphous aluminium alloys, STEM, HRTEM

W niniejszej pracy badano skłonność do tworzenia struktury szklistej oraz strukturę stopów na osnowie Al-Si-Ni. Trzy stopy zostały poddane procesowi odlewania na wirujacy walec miedziany: $Al_{78}Si_{12}Ni_{10}$ [stop 1], $Al_{75}Si_{12}Ni_8Zr_5$ [stop 2] oraz $Al_{73}Si_5Ni_7Cu_8Zr_7$ [stop 3]. Grubość otrzymanych taśm wynosiła pomiędzy 25 a 40 μm. Badania rentgenowskie oraz kalorymetryczne taśm wykazały, że ich struktura jest głównie amorficzna, co potwierdziły metody STEM oraz HRTEM, ujawniając również wydzielenia krystaliczne zidentyfikowane jako roztwór aluminium o wielkości ziarna bliskiej 10 nm. Średnia mikrotwardość [0,1 HV] wyniosła odpowiednio dla stopów 1-3: 457 HV, 369 HV oraz 536 HV. Tak wysoka twardość jest przypuszczalnie związana z obecnością w strukturze amorficznej wydzieleń roztworu α-Al.

1. Introduction

Aluminum based amorphous alloys are now being intensively investigated due to their very good mechanical properties. They show a unique combination of a high tensile strength (even 2-5 times higher than their conventional crystalline counterparts), good resistance to wear and corrosion (due to the absence of grain boundaries) and high elasticity. Amorphous metals derive their strength directly from their non-crystalline structure, which exhibit a different mechanism of deformation with propagation of narrow deformation bands where fine crystalline nuclei are observed [1]. For example, there has been a tensile strength exceeding 1200 MPa reported, which is twice as high as for conventional commercial aluminum alloys [1,2]. Al-based glasses are characterized by low densities of about 3.2-3.7 g/cm^3 what indicate their potential applications in transportation and aviation industry. The first formation of amorphous single phase in Al-based alloys containing more than 50 at.% Al was found in 1981 for Al-Fe-B and Al-Co-B ternary alloys [3] but they did not attract much attention due to their high brittleness. Since then, glass forming ability has been determined in a number of Al – based alloys consisting of Al + transition metal + rare – earth elements (RE), processed mainly by rapid solidification or gas atomization methods [3-8]. Instead of pure RE elements, it is possible to use mischmetals (Mm – combination of different rare – earth elements) which also improves refinement of grains and the ability to amorphize of Al based alloys [9]. However, RE as well as Mm, have a high tendency to oxidation what impedes the production process.

The ductility of glassy aluminum alloys can be improved by their partial crystallization – when a few nanometer size crystals are embedded in the amorphous matrix [1,10]. The strength of these alloys can be increased to over 1400 MPa [11]. Choi et al. [12] reported a tensile fracture strength as large as 1980 MPa for an amorphous alloy containing about 18% Al nanocrystals – this was nearly 1.6 times higher than for the fully amorphous alloy.

Glass forming ability in Al-Si-Ni-Mm alloys was studied by Cieślak in his PhD thesis [9] showing their partial amorphization. In the present paper three Al-Si-Ni based alloys without RE additions were studied, using as a base composition the ternary eutectic AlSiNi after the phase diagram in [13], contrary to hypereutectic alloys investigated in [14]. The compositions were chosen such to consider factors which af-

* INSTITUTE OF METALLURGY AND MATERIALS SCIENCE OF THE POLISH ACADEMY OF SCIENCES, 25 REYMONTA STR., 30-059 KRAKÓW, POLAND
** ICMPE, CNRS UMR 7182, 2-8 RUE HENRI DUNANT, 94320 THIAIS, FRANCE
*** INSTITUTE OF PHYSICS PAS AL. LOTNIKÓW 32/46, PL-02-668 WARSAW, POLAND

fect the glass forming ability (GFA). They include atomic radius differences, enthalpy of mixing and maximum extended solid solubility [1,15]. To amorphize the alloys, the atomic radius of the components has to be significantly different – preferably over 12% – to achieve high packing density and low free volume. Negative heat of mixing of the elements inhibits crystal nucleation. These conditions are fulfilled for close to eutectic AlSiNi composition and even improved in alloys with zirconium addition, due to a reported positive effect of Zr on amorphization behavior of Al based alloys [1,15,16].

2. Experimental procedure

Melt spinning of three Al-based compositions was performed: close to eutectic $Al_{78}Si_{12}Ni_{10}$ [alloy 1], chosen as a base ternary alloy which composition was modified by addition of Zr – $Al_{75}Si_{12}Ni_8Zr_5$ [alloy 2] and Cu with Zr – $Al_{73}Si_5Ni_7Cu_8Zr_7$ [alloy 3] (all in at. %).

The initial ingots were prepared by arc – melting in a purified, Zr – gettered argon atmosphere from a high purity elements (99.9 wt.% and more) and then subjected to a melt spinning process. The alloys were placed in quartz crucibles in an enclosed chamber and then ejected using a He overpressure of 0.2 MPa at a linear speed of a copper wheel of 35 m/s (alloys 1 and 2) and 20 m/s (alloy 3). The mean thickness of the obtained ribbons amounted 33 μm, 25 μm and 42 μm (for alloys 1-3 respectively).

The structure of the ribbons was examined with X – Ray Diffraction (XRD), using Philips PW 1840 diffractometer with Co Kα radiation and Scanning Electron Microscopy SEM using FEI Quanta 3D FEG and Philips XL 30. To examine the microstructure with TEM methods, Titan Cubed 80-300 microscope operated at 300 kV was used. Thin foil specimens were prepared by twin jet electropolishing using 1/3HNO_3 2/3 CH_3OH electrolyte at a temperature about 243 K and voltage of 15V.

Differential Scanning Calorimetry (DSC) studies with Du-Pont and Netzsch thermal analyzers allowed to observe thermal effects in the alloys and determine the crystallization temperatures in the partially amorphous ribbons. Continuous heating of the samples was performed at a rate of 20 K/min. The microhardness of the ribbons was examined with a CSM Instruments Microhardness Tester with a load of 0.1 N.

3. Results and discussion:

Fig. 1 shows a set of diffractograms of alloys 1, 2 and 3, investigated from as cast ribbons. Each of them presents a broad halo characteristic for the amorphous phase. However, alloys 1 and 2 exhibit also strong crystalline peaks identified as resulting from α(Al) solid solution. The peaks are much weaker in alloy 3 which amorphized almost completely.

X – ray diffraction studies confirmed that most of the volume of each cast ribbon is composed of the amorphous phase. The amorphization of these alloys was additionally confirmed by DSC studies, performed at a heating rate of 20 K/s. The curves obtained during thermal analysis are presented in Figs. 2 and 3. The first crystallization peaks, showing maxima at 226°C for alloy 1, 265°C for alloy 2 and 260°C for alloy 3 are of the highest intensity and occur most probably due to the formation of α(Al) solid solution as reported in [9].

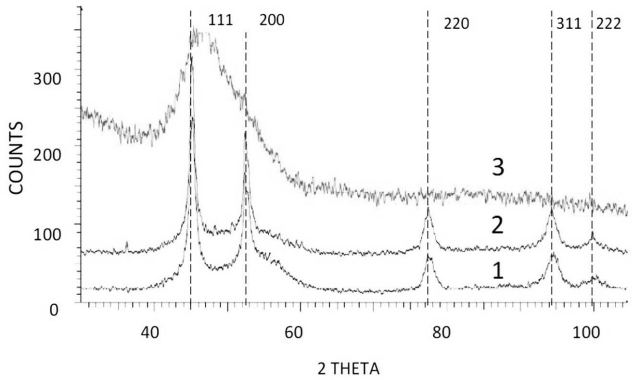

Fig. 1. X – ray diffraction patterns from ribbons made of alloys: 1 - $Al_{78}Si_{12}Ni_{10}$, 2 - $Al_{75}Si_{12}Ni_8Zr_5$ and 3 - $Al_{73}Si_5Ni_7Cu_8Zr_7$

No glass transition effect was observed as also reported for other aluminium alloys [9], however from the increase of the crystallization temperature one can judge that the ΔT_c ($T_L - T_x$) increases for alloys 2 and 3 and therefore also glass forming ability with the addition of a quaternary and quinternary elements [1].

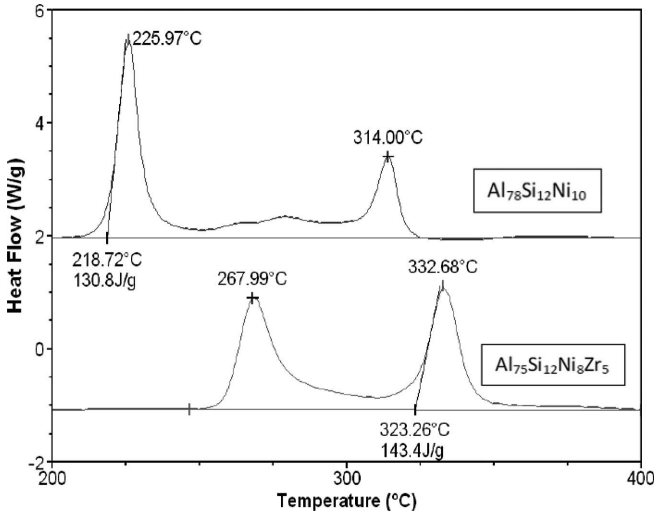

Fig. 2. DSC curves from ribbons obtained from alloys 1 and 2

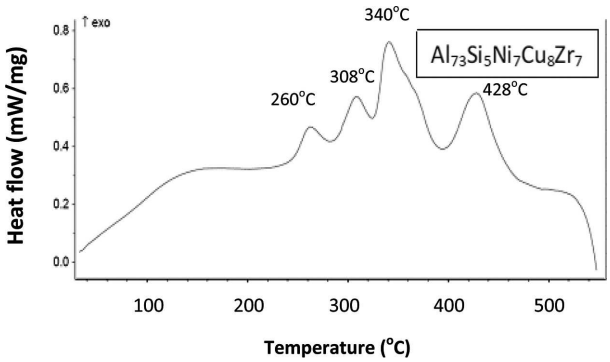

Fig. 3. DSC curve from the ribbon obtained from alloy 3

The DSC curve of the quinternary alloy in Fig.3 presents several peaks starting with the first crystallization peak with

maximum at 226°C and three others at 305°C, 340°C and 430°C. These peaks correspond to crystallization of various phases starting most probably with aluminium solid solution as in the case of alloys 1 and 2 and then formation of various intermetallic phases. The total enthalpy of the exothermal effects is of alloy 1 is about 131 J/g. The curve for the quaternary alloy presents only two exothermal peaks near 268°C and 333°C with the enthalpy about 143 J/g.

In order to study the microstructure of the ribbons in the as cast condition SEM and TEM methods were applied. SEM image of alloy 1 is presented in Fig. 4. It shows a part of the ribbon with crystalline particles of size of a few hundred nm seen as brighter particles in a grey matrix. Larger crystalline particles can be observed in the SEM micrograph taken from alloy 2. They are of 300 nm - 2 μm size and located near the surface, since the bottom part of the ribbon at the copper wheel side with a higher cooling rate does not show crystalline particles.

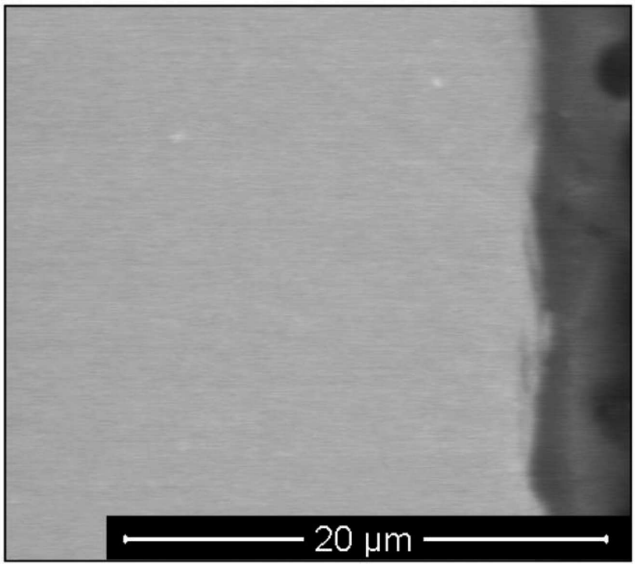

Fig. 4. SEM micrograph of alloy 1

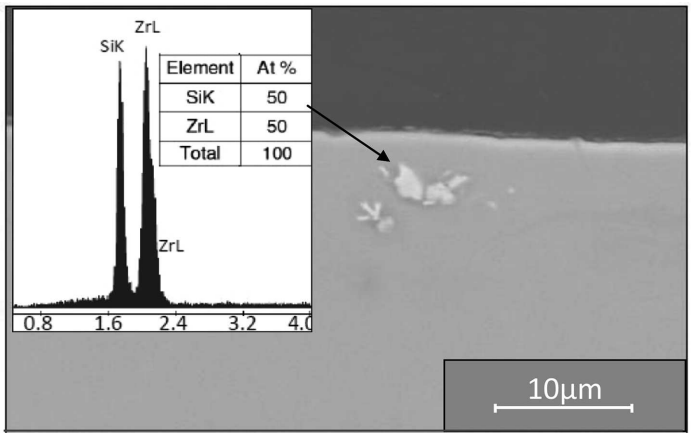

Fig. 5. SEM image of ribbon 2 ($Al_{75}Si_{12}Ni_8Zr_5$ alloy) with EDS analysis of the bright inclusions

EDS technique allowed to check the composition of these crystallites and the results indicated the presence of Si-Zr compounds. Similar investigations were conducted for alloy 3. In that ribbon some primary crystallites were found as well, yet their morphology showing elongated shape was different, most probably due to a different chemical composition – Fig. 6.

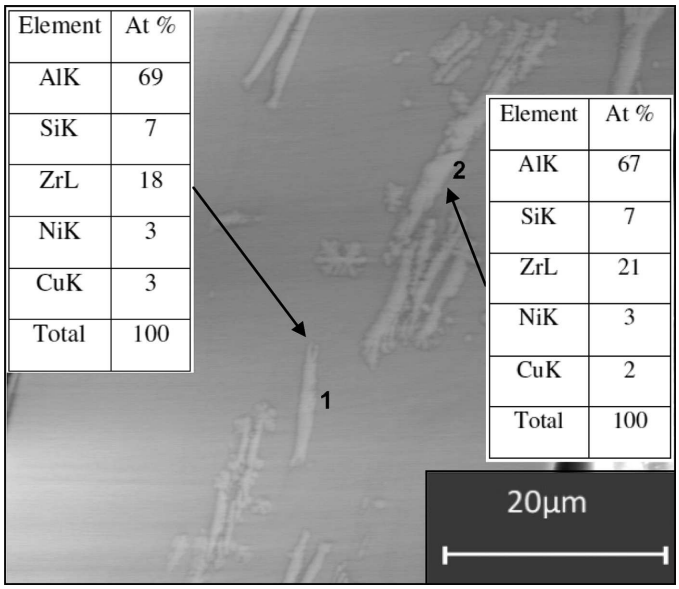

Fig. 6. SEM image of ribbon 3 ($Al_{73}Si_7Ni_7Cu_8Zr_7$ alloy)

Taking into account that point EDS analysis of inclusions is modified by matrix lying beneath them, the results may indicate the presence of Al_3Zr phase with a small amount of some other solute elements. SEM studies indicated a different mode of crystalline particles in the ternary and multicomponent alloys, where crystalline inclusions become coarser with increasing number of alloying elements.

In order to observe the fine structure of crystalline particles and ordering within the amorphous matrix, advanced TEM methods like High Resolution Transmission Electron Microscopy (HRTEM) and Scanning Transmission Electron Microscopy (STEM) were applied. Fig. 7a presents STEM microstructure of the ribbon from alloy 1. The microanalysis shows a difference in the chemical composition between the bright and grey areas. The phase seen in brighter contrast contain Al71Si14Ni15 (in at%) i.e. composition similar to the initial one, while the darker areas are enriched in Si at the expense of aluminium.

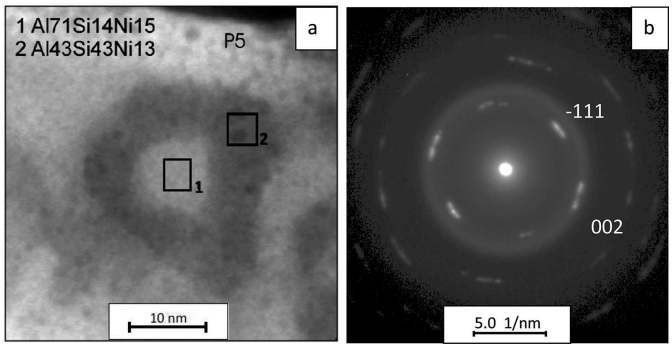

Fig. 7. STEM image of ribbon 1 with chemical composition EDS analysis from the marked areas and SADP from a darker part of the ribbon in [110] zone axis orientation

Selected Area Diffraction Pattern (SADP) from the part of the matrix with many darker areas shows reflections from

α(Al) solid solution in [110] zone axis orientation diffused around Debye-Scherrer rings (Fig. 7b). It indicates a relatively strong texture of crystallites due to their direction of growth determined by the heat conduction. The matrix of the ribbon visible as brighter is amorphous, as can be seen in Fig. 8. HRTEM image shows absence of crystalline phase or short range order as supported by the Fast Fourier Transform (FFT) (picture shown as an insert). The FFT image presents perfectly round, broadened halo without any additional reflections what indicates perfectly amorphous structure without any crystalline contrast, similar to that observed in perfect amorphous structures [1].

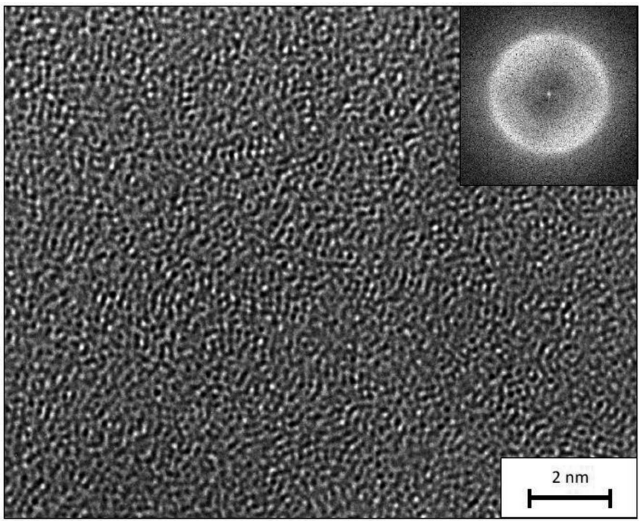

Fig. 8. HRTEM of the ribbon from alloy 1 with FFT (Fast Fourier Transform) image from the area – presented in the micrograph as an insert

Similarly to ribbon 1, the composition of ribbon 2 is not homogeneous as can be seen in the STEM image in Fig. 9. One can see some brighter areas which form the matrix and darker zones enriched in alloying elements at the expense of Al content (as results from EDS spectra in Fig. 9), where most probably crystalline elements exist similarly like in alloy 1.

TEM observations confirmed also the existence of α-Al phase which was revealed by XRD studies. Fig. 10 presents a typical HRTEM from the ribbon of alloy 2. It shows almost perfect amorphous structure, however weak fringes corresponding to {220}lattice planes (well visible in the upper right corner) can also be seen. The FFT from this area presents broad rings due to random positions of atoms in the amorphous phase, simultaneously with points from lattice fringes indicating the presence of α(Al) crystals in [-111] zone axis orientation. Transmission electron microscopy studies allowed to detect a lack of short range ordering in the amorphous structure and in addition the presence of lattice fringes due to the nanocrystalline particles of α(Al) embedded in the amorphous matrix. Some other crystals could not be identified as aluminum solid solution being most probably intermetallic phases.

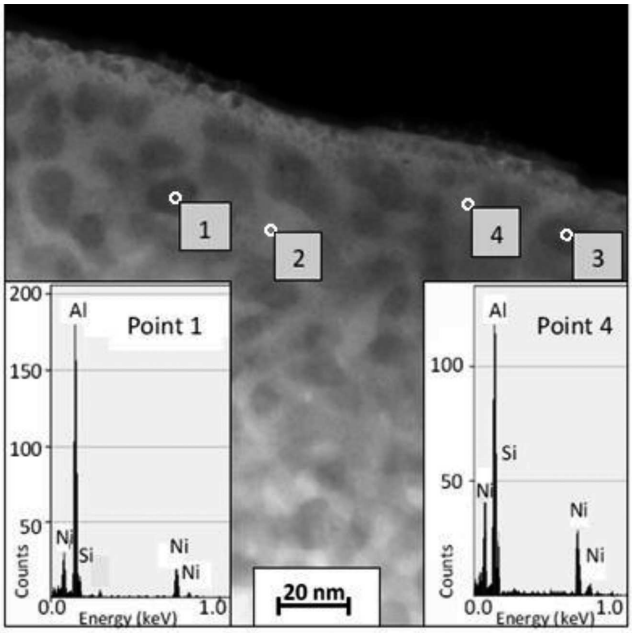

Fig. 9. STEM image of ribbon 2 with composition analysis from the marked areas

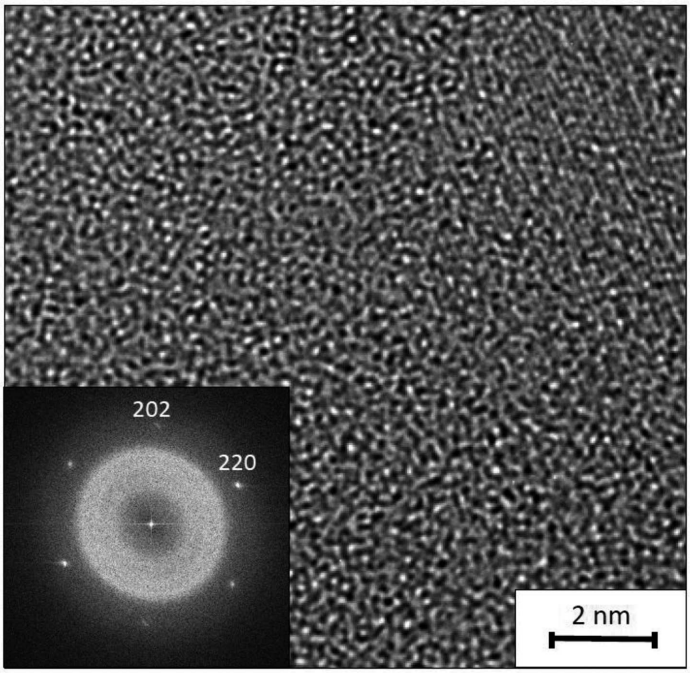

Fig. 10. HRTEM image from ribbon 2 with FFT in [-111] zone axis orientation

The ribbons were examined also in terms of their microhardness and the results are presented as a graph in Fig. 11. The experiments revealed that all of the ribbons were very hard as compared with the crystalline counterparts of the alloys. Surprisingly, the hardness of ribbon 2 (369 HV 0.1) was lower than for ribbon 1 – without the addition of Zr (457 HV 0.1). However, the addition of both Zr and Cu resulted in the highest value of this property in ribbon 3 (535 HV 0.1). This was most probably due to highest fraction of the amorphous phase as resulted from the X-ray diffraction studies.

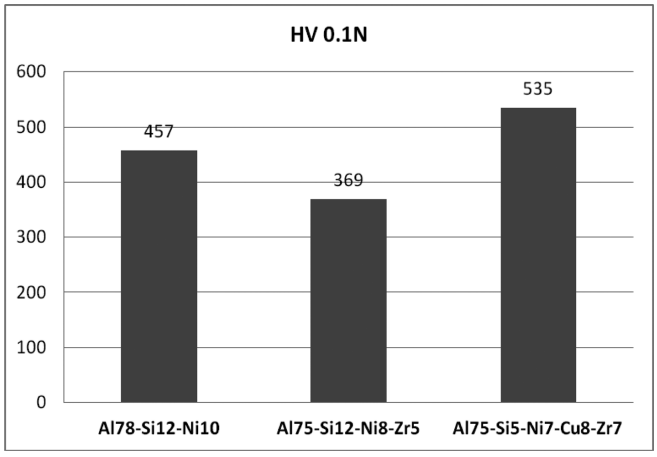

Fig. 11. The histogram of microhardness of ribbons 1-3 respectively

4. Conclusions

1. Melt spinning of the Al-Si-Ni based alloys leads to predominantly amorphous structure with fine inclusions of α(Al) phase containing less solute elements than the amorphous phase. The addition of Zr and Cu causes increased fraction of the amorphous phase, however the crystalline particles become coarser.
2. The addition of Zr and Cu to Al-Si-Ni system increases the value of microhardness of melt spun ribbons up to 535 $HV_{0.1}$ what is nearly 80 HV more than for the initial ternary alloy. It is most probably caused by increased fraction of the amorphous phase in the ribbons and a different shape of crystalline particles.
3. The crystallization in the investigated ribbons proceeds as a multistage process manifested by a few exothermal peaks appearing during the continuous heating. The addition of Zr and Cu to the ternary AlSiNi alloy causes an increase of the start crystallization temperature of melt spun ribbons of about 40°C.

Acknowledgements

The financial support from the research grant 2011/01/M/ST8/07828 and Pollonium 8415/2011 is gratefully acknowledged.

Received: 20 January 2013.

REFERENCES

[1] C. Suryanarayana, A. Inoue, Bulk Metallic Glasses, CRC Press, Boca Baton, 382 (2012).
[2] M. Gogebakan, P.J. Warren, B. Cantor, Materials Science and Engineering **A226-228**, 168-172 (1997).
[3] A. Inoue, Prog. Mater. Sci. **43**, 365-520 (1998).
[4] A. Inoue, Y. Kawamura, Y. Kimura, H.M. Mano, Mater. Sci. Forum **360-362**, 129-136 (2001).
[5] W.T. Kim, M. Gogebakan, B. Cantor, Materials Science and Engineering **A226-228**, 178-182 (1997).
[6] C.R.M. Afonso, C. Bolfarini, C.S. Kiminami, N.D. Bassim, M.J. Kaufman, M.F. Amateau, T.J. Eden, J.M. Galbraith, Journal of Non-Crystalline Solids **284**, 134-138 (2001).
[7] X.C. Tong, H.S. Fang, Materials Letters **28**, 133-136 (1996).
[8] K.R. Cardoso, A.G. Escorial, W.J. Botta, F., Journal of Non-Crystalline Solids **273**, 266-270 (2000).
[9] G. Cieślak, Wytwarzanie nanokrystalicznych stopów z układu Al-Si-Ni-Mm (miszmetal). PhD thesis, Politechnika Warszawska, Warszawa 2012.
[10] D.H. Kim, W.T. Kim, D.H. Kim, Materials Science and Engineering **A385**, 44-53 (2004).
[11] Y. Kawamura, H. Mano, A. Inoue, Scripta Mater. **44**, 1599-1604 (2001).
[12] G.S. Choi, Y.H. Kim, H.K. Cho, A. Inoue, T. Masumoto, Scripta Met. et Mat. **33**, 1301-1306 (1995).
[13] P. Villars, A. Prince, H. Okamoto, Handbook of Ternary Alloy Phase Diagrams, ASM Int., Ohio, p. 4167 (1995).
[14] B.J. McKay, P. Cizek, P. Schumacher, K.A.Q. O'Reilly, Materials Science and Engineering **A304-306**, 240-244 (2001).
[15] L. Wang, L. Ma, H. Kimura, A. Inoue, Materials Letters **52**, 47-52 (2002).
[16] J. Dutkiewicz, A. Kukuła, L. Lityńska-Dobrzyńska, A. Góral, Int. J. Mat. Res. **103**, 9-12 (2012).